Journal of Photochemistry and Photobiology A: Chemistry 353 (2018) 325–336

Contents lists available at ScienceDirect

Journal of Photochemistry and Photobiology A: Chemistry

journal homepage: www.elsevier.com/locate/jphotochem

CeO_2/TiO_2 nanostructures enhance adsorption and photocatalytic degradation of organic compounds in aqueous suspension

Gabriela Bonfanti Vieira[a], Humberto Jorge José[a], Michael Peterson[b], Vanessa Zanon Baldissarelli[c], Pedro Alvarez[d], Regina de Fátima Peralta Muniz Moreira[a,*]

[a] Laboratory of Energy and Environment, Department of Chemical and Food Engineering, Federal University of Santa Catarina, Florianópolis 88040-900, Santa Catarina, Brazil
[b] Department of Chemical Engineering, University of the Southern end of Santa Catarina, Criciúma 88806-000, Santa Catarina, Brazil
[c] Department of Chemistry, Federal Institute of Education, Science and Technology of Santa Catarina, Araquari 89245-000, Santa Catarina, Brazil
[d] Department of Civil and Environmental Engineering, Rice University, Houston 77005, TX, United States

ARTICLE INFO

Article history:
Received 29 July 2017
Received in revised form 10 November 2017
Accepted 24 November 2017
Available online 26 November 2017

Keywords:
Cerium
Morphology
Adsorption
Reactive oxygen species
Photosensitization

ABSTRACT

Mixed oxide interfaces are critical in the delivery of active components in photocatalytic processes. Cerium doped TiO_2 photocatalysts were prepared using a hydrothermal route to manipulate the morphology of the photocatalyst and improve the interaction between CeO_2 and TiO_2 nanoparticles. These changes were compared with the photocatalytic activity and adsorption capacity of the solids. The photocatalysts were used to degrade polyvinylpyrrolidone (PVP) and methylene blue (MB) as test compounds. A low photodegradation rate of PVP (0.0001 min^{-1} and 0.0005 min^{-1} under visible and UV light, respectively) was observed using Ce-doped photocatalysts, with no adsorption. The high adsorption capacity of MB (34.46 mg g^{-1}) proved that the local morphology of the nanostructured CeO_2/TiO_2 photocatalysts is more important than the amount of CeO_2 in the sample, and the main role of the CeO_2 on mixed photocatalysts is to improve thermal stability during the synthesis. XRD, XPS, BET surface area, UV–vis and TEM techniques confirmed this conclusion. The rate of degradation of MB by the Ce-doped photocatalyst decreased dramatically when using the singlet oxygen scavenger L-Histidine (0.0214 min^{-1} to 0.0001 min^{-1}), indicating a photocatalysis sensitized by the dye, under visible and UV light.

1. Introduction

Photocatalysts are materials that can accelerate chemical reactions by absorbing light quanta of suitable wavelengths depending on the band structure [1]. Among photocatalysts, titanium dioxide is widely used because of the advantageous balance between its surface-chemistry-related properties and the physical properties required for efficient handling of light-trigged charge carriers, which allows them to be involved in chemical reactions at the surface [2,3].

Nevertheless, the TiO_2 activity is still insufficient for most large scale applications and robust systems with broad application must be produced for complete degradation of all types of pollutants and that can function in all experimental conditions [4,5]. To overcome these drawbacks, numerous approaches have been employed over the past several decades, including the coupling of TiO_2 with a second metal oxide to obtain high activity photocatalysts.

Anionic or cationic doping of TiO_2 in both interstitial and substitutional sites of the TiO_2 crystal can lead to a substantial change in the density of electronic states (DOS) near the Fermi level [6]. First-principles Density Functional Theory (DFT) studies have shown that cationic doping of TiO_2 causes the appearance of new energy levels in the band gap, which is in agreement with the experimentally observed decrease of apparent band gap and coloration of TiO_2 [6–8]. However, despite the decrease in the band gap energy and enhanced optical absorption, cationic doped TiO_2 frequently exhibits lower photocatalytic efficiency than pristine TiO_2, since cationic impurities can also act as traps as well as recombination centers for the generated carriers [6].

The modification of TiO_2 by doping with rare earth metals has been proposed to increase the photocatalytic activity by reducing the band gap, improving charge separation (electron/hole), and/or increasing the adsorption capacity [9,10]. Furthermore, there are few reports of visible light photocatalysis using lanthanide-doped TiO_2.

* Corresponding author.
E-mail address: regina.moreira@ufsc.br (R. de Fátima Peralta Muniz Moreira).

https://doi.org/10.1016/j.jphotochem.2017.11.045
1010-6030/

The use of CeO_2 has been extensively investigated in many catalytic processes due to its low cost, abundant supply, unique redox chemistry ($Ce^{4+} \leftrightarrows Ce^{3+}$ easily interchangeable) and its oxygen storage/transport and activation properties [11]. The photocatalyst Ce-doped TiO_2 frequently has a lower band gap than TiO_2, depending on the Ce content and the method used to prepare the coupled-photocatalyst [12–14], which allows it to be activated by visible light. The photocatalytic activity of Ce-doped TiO_2 depends on the Ce content, and usually achieves a maximum when Ce content is in the range of 0.025–0.6 mol% [2,5,13,15,16]. Depending on the ceria loading, the interaction between the two metal oxides could lead to unusual coordination modes, and the interaction of the CeO_x nanoparticles would increase as the Ce content decreases [11,17]. However, some authors have reported a strong suppressive effect when cerium is present in high concentrations in TiO_2 [18,19]. The inhibitory effect could be related to the presence of unpaired electrons in the 4*f* orbital of Ce that can effectively capture the photogenerated electrons and holes, thereby preventing their diffusion to the TiO_2 surface, which significantly reduces photocatalytic activity.

Although several studies exist, the relationship between the structure and activity of CeO_2/TiO_2 photocatalysis is still not completely understood. Only a few articles describe what happens in the CeO_2/TiO_2 interface under irradiation. An intermixed solid solution can only form when Ce is the predominant component, while separated phases of ceria and titania co-exist when CeO_x is a minor component. However, although CeO_2/TiO_2 should exhibit excellent redox properties, it has difficulty forming solid solutions and the realization of these properties depends on the ability to prepare metastable material structures [20].

The identification of Ce^{3+} on the surface of CeO_x/TiO_2 could be related to the formation of electron-hole pairs under visible light irradiation and improvement of the photocatalytic activity [2]. The Ce^{3+} ions are larger than the Ce^{4+} ions and the formation of Ce^{3+}-vacancy clusters distorts the surrounding fluorite lattice. In fact, the presence of reduced Ce^{3+} on the surface appeared to be key to understanding the photocatalytic activity, since Ce^{3+} states may alter the fluorite conduction band and allow the efficient location of TiO_2 conduction band electrons that are generated after photoexcitation. Thus, the CeO_2/TiO_2 interface has a critical role in the photocatalytic activity, and the contact between CeO_2 and TiO_2 influences the activity by promoting effective separation of charge and leaving hole species available for chemical reaction.

Nevertheless, all of the photocatalytic applications have in common the fact that a higher overall reaction rate is achieved using high surface area geometries. Hierarchical TiO_2 materials have been employed to extend the photocatalytic activity due to its specific structure, high surface area, adjustable crystallinity and the short diffusion distance of e^-/h^+ pairs [21]. The preparation approaches for structuring TiO_2 materials are extensive, including hydrothermal treatment [22], microemulsion [23], sol-gel [21] and evaporation-induced self-assembly [23] etc.

In this paper, we used the CeO_2/TiO_2 system to investigate the role of the photocatalytic composite material CeO_2/TiO_2 interface on the photocatalytic degradation of organic compounds under visible and UV light.

2. Experimental

2.1. Preparation of TiO_2 photocatalysts

TiO_2 P25 (80% anatase and 20% rutile) was purchased from Degussa Co. $Ce(NO_3)_3$ was obtained from Sigma Aldrich. Analytically pure NaOH and HCl were used in the experiment. All of these chemicals were used without further purification. Distilled water was used in these experiments.

The TiO_2 photocatalysts were prepared by a hydrothermal method [24,25]. Briefly, 60 mL of an aqueous solution of 10 M NaOH and 3 g of TiO_2 P25 were used. The mixture was subjected to magnetic stirring for 1 h until complete homogenization occurred. The solution was then transferred to a steel autoclave coated with polytetrafluorethylene and placed in an oven at 120 °C for 24 h. After the reaction under controlled temperature, sodium was removed by filtering and washing with a 0.1 M HCl solution and distilled water until the pH became neutral. The material was dried at 60 °C and calcined at 450 °C or 600 °C for 2 h at a heating rate of 10 °C min^{-1}.

The TiO_2 phase transformation from anatase to rutile is observed between 500 and 600 °C, and then completely transformed to the rutile phase at 600 °C [26–28], while the cerium nitrate decomposition to form cerium oxide occurs in the range of 200 to 300 °C [29]. Therefore, temperatures in the range of 450 to 600 °C ensure the complete decomposition of cerium nitrate, thus maintaining the crystalline phase distribution anatase/rutile during the synthesis.

The Ce-doped photocatalysts were prepared using similar procedures and by adding $Ce(NO_3)_3$ to the autoclave. Different amounts of Ce were added during the first step along with NaOH and TiO_2-P25, in order to attain CeO_2/TiO_2 with different cerium molar content (0%, 0.09%, 0.29% and 0.57% mol). The nomenclature of the samples is shown in Table 1.

2.2. Characterization of the TiO_2 photocatalysts

The crystalline properties of the samples were characterized by X-ray diffraction (XRD, Philips X'Pert) performed at room temperature using Cu Ka radiation at 40 kV and 30 mA (geometry $\theta - 2\theta$ and $\lambda = 1.54056$ Å). The morphology of the photocatalysts and the particle size were analyzed by transmission electron microscopy (JEM-2100 TEM). The Brunauer–Emmett–Teller (BET) surface area was determined by nitrogen adsorption measurement at 77 K (Quantachrome Autosorb-1 model). Prior to analysis, the samples were heated to 100 °C for 12 h to desorb any adhering molecules and remove moisture from the sample. Band gap values were obtained using a UV–vis diffuse reflectance spectrophotometer (Perkin Elmer UV/vis/NIR Lambda 750). The zeta potential of the photocatalysts prepared were measured using a Stabino® Particle Charge Mapping analyzer (Particle Metrix, Germany). For surface analysis and cerium valence state analyses, X-ray photoelectron (XPS) spectra were taken using a VG ESCA 3000 system and Al Kα radiation with overall energy resolution of approximately 0.8 eV. The energy scale was calibrated using the Fermi level and C1s peak at 284.5 eV. The spectra were normalized to maximum intensity after a constant background subtraction.

Table 1
Designation of photocatalysts prepared in this work.

Sample	% Ce mol	Temperature of Thermal treatment, °C
TiO_2-P25	–	–
TiO_2-450	–	450
TiO_2-600	–	600
0.09Ce-TiO_2-450	0.09	450
0.09Ce-TiO_2-600	0.09	600
0.29Ce-TiO_2-450	0.29	450
0.29Ce-TiO_2-600	0.29	600
0.57Ce-TiO_2-450	0.57	450
0.57Ce-TiO_2-600	0.57	600

2.3. Photocatalytic activity – kinetics of PVP degradation and MB decolorization in a slurry reactor

To evaluate the photocatalytic activity, methylene blue (MB) and polyvinylpirrolidone (PVP) were selected. The photocatalytic decomposition of the first compound has been extensively studied, and the degradation mechanism could also include photocatalysis and photosensibilization [30–32]. On the other hand, polyvinylpyrrolidone is hardly degraded by the TiO_2/UV process in aqueous solution [33].

The photocatalytic experiments were performed in a jacketed annular photoreactor (1 L), equipped with a visible light (400–800 nm) or a medium-pressure mercury vapor lamp (model HQL E27 OSRAM; the wavelength range is from 200 nm to 800 nm with a maximum emission at 368 nm; 41 W m^2 measured illumination intensity), at 20 °C.

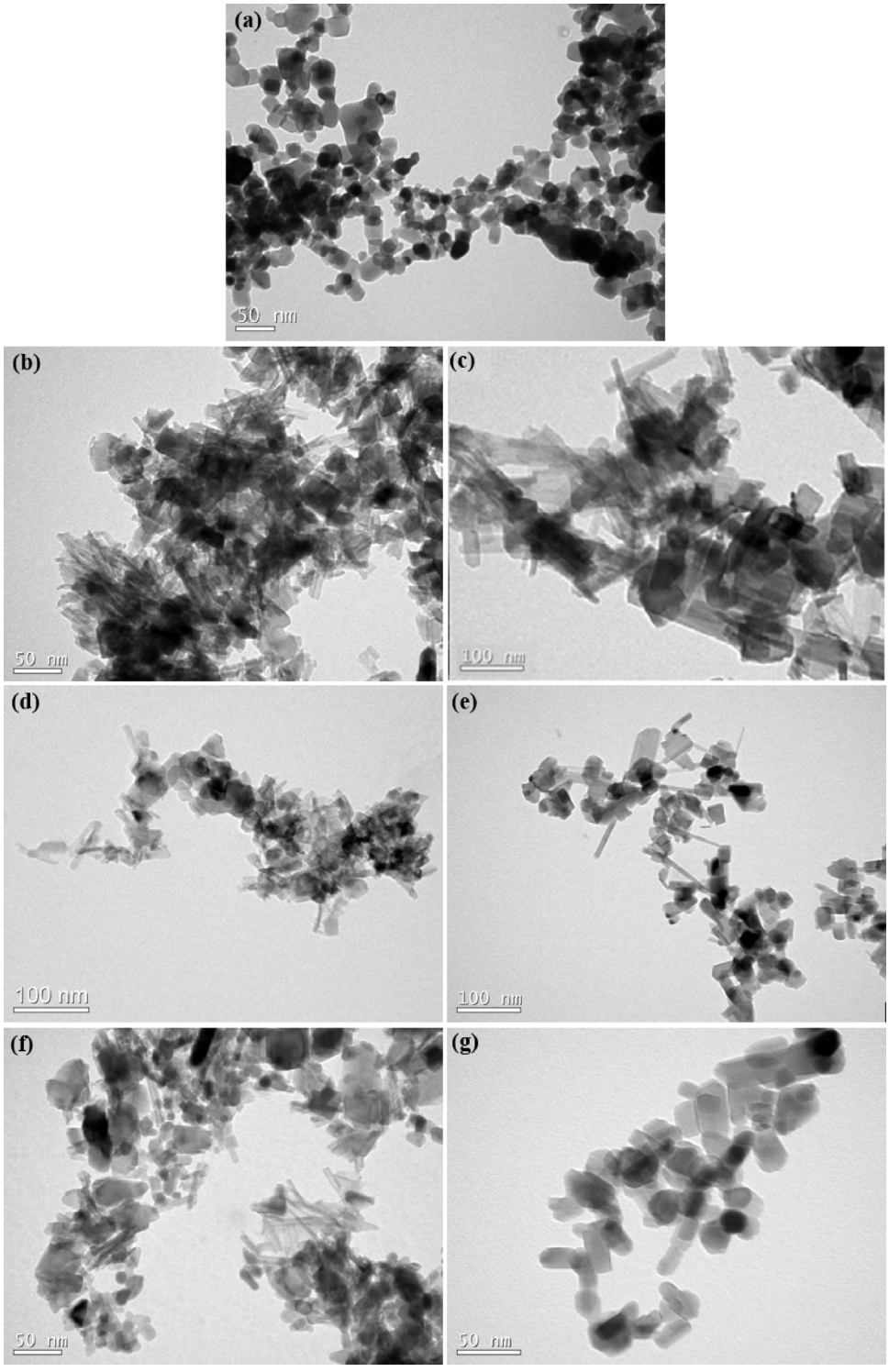

Fig. 1. TEM images of photocatalysts: (a) TiO_2-P25, (b) TiO_2-450, (c) TiO_2-600, (d) 0.29Ce-TiO_2-450, (e) 0.29Ce-TiO_2-600, (f) 0.57Ce-TiO_2-450 and (g) 0.57Ce-TiO_2-600.

Before the photocatalytic reactions, the aqueous solution containing PVP (300 mg L^{-1}) or MB (20 mg L^{-1}) and the photocatalyst (500 mg L^{-1}) were agitated in dark conditions until adsorption equilibrium was reached. The PVP or MB concentrations were measured at set times and the equilibrium of adsorption was defined when the concentration remained constant over time. The lamp was then turned on and air was pumped to the aqueous suspension at a flow rate of 0.168 L min^{-1}. The mixture received constant magnetic stirring at 1000 rpm. Aliquots were collected at set times, filtered through a GV membrane (Durapore) PVDF (0.22 μm) and the total organic carbon (TOC) was measured using a TOC analyzer (Shimadzu TOC-V_{CPH}). The decolorization of MB was accomplished by UV–vis spectrophotometry (HACH DR5000).

The percentages of TOC removal (to PVP) and color removal (to MB) were calculated according to Eqs. (1) and (2) respectively:

$$TOCremoval(\%) = \frac{TOC_0 - TOC_t}{TOC_0} \times 100 \quad (1)$$

$$Color\ removal(\%) = \frac{A_0 - A_t}{A_0} \times 100 \quad (2)$$

where TOC_0 and TOC_t are initial TOC and TOC after irradiation at various time intervals, respectively. A_0 and A_t are initial absorbance, and the absorbance after irradiation at various time intervals, respectively. The PVP mineralization rate constant ($k_{1\text{-}PVP}$) or MB decolorization rate constant ($k_{1\text{-}v}$) were obtained according to pseudo-first-order rate laws based on volume ($k_{1\text{-}v}$) or based on photocatalyst mass ($k_{1\text{-}w}$), which can be expressed by Eqs. (3) and (4), respectively:

$$ln(TOC_0/TOC_t) = k_{1-PVP}t \quad (3)$$

$$\ln(A_0/A_t) = k_{1-v}t \quad (4)$$

where $k_{1\text{-}v}$ is the MB decolorization pseudo-first-order rate constant (min^{-1}) based on volume; and $k_{1\text{-}PVP}$ is the PVP mineralization pseudo-first-order rate constant (min^{-1}). The pseudo-first-order rate constant based on the solid weight is given by Eq. (5):

$$k_{1-w} = k_{1-v}/w \quad (5)$$

where w is the photocatalyst dosage (g L^{-1})

By plotting ln (TOC_0/TOC_t) or ln (A_0/A_t) versus time, the slope of the straight line gives the first-order rate constant for PVP mineralization or MB decolorization, respectively ($k_{1\text{-}PVP}$, $k_{1\text{-}v}$ or $k_{1\text{-}w}$).

2.4. Determination of ROS generated by TiO_2 photocatalysts under visible and UV light

To determine the reactive oxygen species that act on the photodegradation of PVP and MB, the methodology used radical scavengers to evaluate the pure TiO_2 photocatalyst and that doped with cerium with the highest photocatalytic performance. L-Histidine or sodium azide were used as a singlet oxygen ($^1O_2$) scavenger, dimethylsufoxide (DMSO) or sodium carbonate were used as the hydroxyl radical ($^{\bullet}OH$) scavenger. All the scavengers were used in the same concentration, 5 mM.

3. Results and discussion

3.1. Morphology change of TiO_2-P25 before Ce doping by hydrothermal method

The hydrothermal method for TiO_2 synthesis usually produces hierarchical nanostructures, such as nanosheets, nanowires or nanotubes, depending on the experimental conditions. During synthesis, nanosheets can grow up to a sufficient reaction temperature and subsequently envelop themselves, and transform into nanotubes due to the high energy state, producing elongated structures as shown in Fig. 1. This transformation can be hindered if there is insufficient agitation in the Teflon reactor during the hydrothermal route [34–36].

It can be seen that the photocatalysts prepared in this work have a nanometric size (below 100 nm) with varied morphology in nanoparticles, nanosheets and nanotubes. The samples calcinated at 600 °C produced nanoparticles with higher dimensions and an absence of nanotubes.

It can be observed that the length of the nanotube decreased as the doping ratio increased, suggesting a new form of structure of the clusters, which is not found in the TEM result of the undoped samples.

3.2. BET surface area and band gap of TiO_2 photocatalysts

It has been frequently reported that Ce doped TiO_2 prepared by the hydrothermal or sol-gel, method presents a high surface area [14,16,34]. The S_{BET} of the TiO_2–450 °C or doped photocatalysts calcined at 450 °C was higher than that of TiO_2-P25, but the S_{BET} decreased with increasing calcination temperature for all doped and undoped photocatalysts (Table 2). The increase in the calcination temperature causes a narrowing of the morphology, where the particles are more compact, reducing the surface area. At each calcination temperature, the doped material had a larger S_{BET} than the undoped material. However, the BET surface area decreases as the Ce content increases, suggesting a possible loss of

Table 2
BET surface area, cerium surface density, point of zero charge, band gap and crystallite size for different photocatalysts.

Photocatalysts	S_{BET} ($m^2\ g^{-1}$)	Ce_{sd} (Ce atom nm^{-2})	pH_{pzc}	E_G (eV)	Crystallite size (nm)
TiO_2-P25	50.10	–	6.3	3.20	20.75
TiO_2-450	80.28	–	3.1	3.24	14.31
TiO_2-600	47.25	–	3.2	3.25	19.77
0.09Ce-TiO_2-450	92.53	6.97	a	a	18.54
0.09Ce-TiO_2-600	45.66	14.12	a	a	17.95
0.29Ce-TiO_2-450	107.90	19.92	3.8	3.25	17.30
0.29Ce-TiO_2-600	53.57	40.13	3.5	3.23	17.30
0.57Ce-TiO_2-450	73.19	58.74	3.7	3.21	19.77
0.57Ce-TiO_2-600	56.61	75.94	4.8	3.24	15.97

a. not measured.

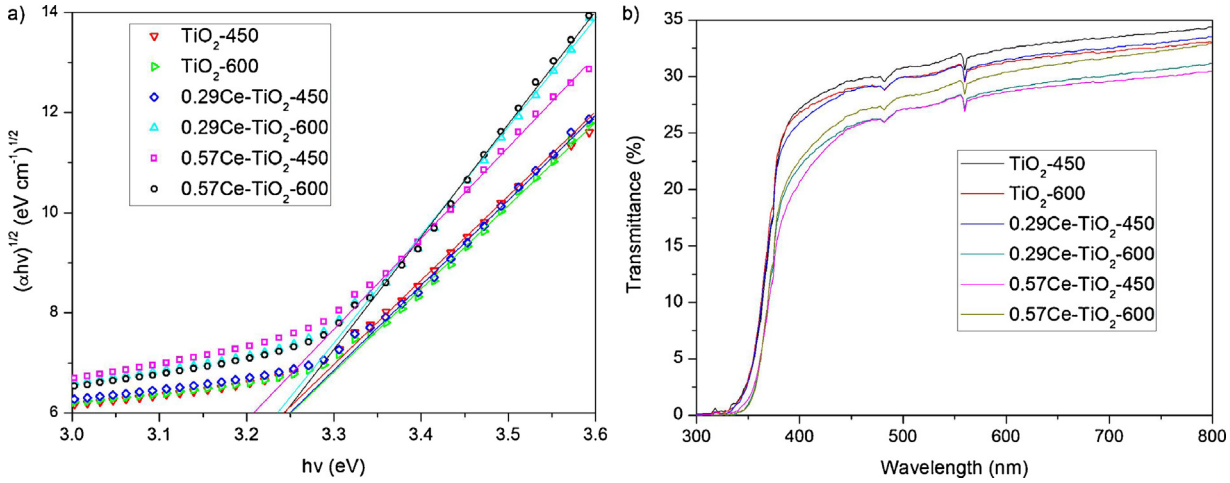

Fig. 2. Tauc's plot: αhv as a function of photon energy (a) and UV–vis transmission spectra (b) for pure or Ce doped TiO_2 photocatalysts.

contact between CeO_2 and TiO_2 [2,37]. Therefore, it would be expected that the sample 0.29Ce-TiO_2-450 has the highest contact between ceria and titania.

The Ce surface density of each sample show us the quantity of Ce per unit area distributed over the surface of the materials and is obtained by Eq. (6) [38]:

$$Ce_{sd} = \frac{\%\text{mass of Ce} \times A}{S_{BET} \times MM_{Ce}} \quad (6)$$

where the Ce_{sd} is expressed as the number of Ce atoms per square nanometer of surface area (Ce atom nm^{-2}); %mass of Ce is the nominal mass percentage of Ce doped; A is Avogadro's number; S_{BET} is the surface area ($nm^2\,g^{-1}$) and MM_{Ce} is the molar mass of the Ce ($mol\,g^{-1}$).

Table 2 indicates that the Ce surface density depends on the amount of Ce doped and the BET surface area, and decreases as the calcination temperature increases.

The band gap values (E_G) of the photocatalysts (see Table 2) were estimated by diffuse reflectance spectroscopy and the Kubelka-Munk equation [39]. Doping TiO_2 with Ce did not significantly change the band gap of the photocatalysts. In fact, the expected decrease on the band gap with Ce doping was only observed using a CeO_2 content higher than 1 mol% [14].

According to Huang et al. [40], oxygen vacancies could shorten the band gap of pure CeO_2 and enhance the absorption of visible light because it is easier to Ce^{3+} created by generation of oxygen vacancies than Ce^{4+} under same irradiation. These oxygen vacancies generated would lead to higher visible light absorption and less electron-hole recombination on the surface of the particles, which qualitatively matched the computational results.

However, as the surface area decreased with the cerium content, it would be expected that contact at the CeO_2/TiO_2 interface would decrease because of the formation of clusters on the solid surface. DFT simulations have indicated that the cluster size (or coverage) affects the catalytic activities of MOx/TiO_2 [41].

The UV–vis spectra (Fig. 2b) shows the influence of cerium doping on the UV–vis absorption of the photocatalysts. It indicates that the optical absorption in the 200–300 nm range for CeO_2/TiO_2 doped with various cerium contents is almost the same, but the light absorption in the visible region is different. Cerium doping in TiO_2 causes a redshift in the absorption spectra, and the light absorption increases with an increasing amount of cerium in the range of 400–800 nm. The results indicate that cerium doping enhances the light utilization efficiency. The redshift in the absorption spectra is interpreted as possible evidence of a good contact between TiO_2 and the cerium species, which indicates the presence of Ti—O—Ce bonds.

Futhermore, besides having nearly the same band gap, TiO_2-450 and 0.29Ce-TiO_2-450 had the same photoluminescence intensity (results not shown), indicating the same recombination of photoexcited electrons and holes.

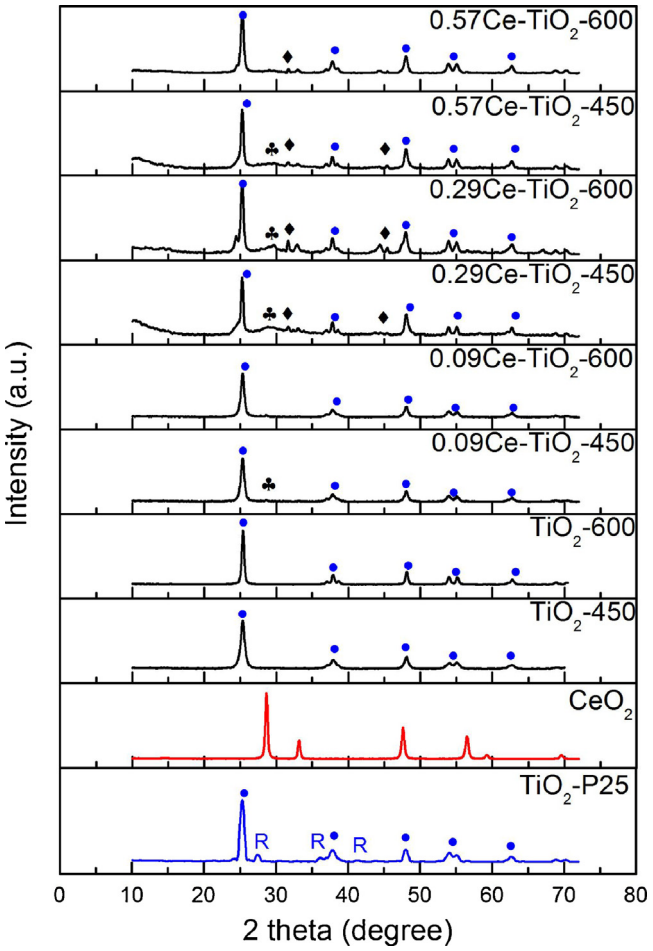

Fig. 3. XRD patterns of CeO_2 and all the photocatalysts prepared. The symbols ●, R, ◆ and ♣ indicate anatase TiO_2, rutile TiO_2, NaCl and $Na_2Ti_9O_{19}$, respectively.

3.3. Cristalinity of TiO_2 photocatalysts by XRD

XRD (Fig. 3) revealed the presence of anatase on all the doped and undoped samples. Even at 600 °C, the dominant crystalline phase was anatase. The diffraction peaks at 2θ values of 25.17°, 37.60°, 47.76°, 54.01°, and 62.60° are indexed to the (101), (004), (200), (105) and (204) planes of the anatase phase of TiO_2 [42]. In the presence of Ce, the crystallinity of the material remained unchanged with an increasing calcination temperature [13].

The absence of cerium oxide in XRD patterns can be attributed to the small percentage in the samples. Another reason may be that the cerium species are successfully doped into the lattice of TiO_2, or well dispersed, as small particles of CeO_2, on the surface of TiO_2 with a low Ce content not detected by the XRD technique [43].

Because the ionic radius of Ce^{4+} and Ce^{3+} are 0.093 and 0.103 nm, respectively, larger than that of Ti^{4+} which is 0.068 nm, it is difficult for doped cerium ions to enter into the TiO_2 lattice [14]. The cerium species may remain on the surface of the TiO_2 [44], and the doping cerium may be present as the so-called second phase on the surface of the TiO_2.

Ti^{4+} ions easily enter into the crystal lattice of rare earth oxides, and even substitute the rare earth ions [45], which then form Ti—O—Ce bonds. The second phase suppresses the crystallite growth of the rutile phase and this could explain why the phase transformation from anatase to rutile is inhibited in the Ce doped samples after thermal treatment even at 600 °C [15,46].

In some samples, peaks occurred at 31.65° and 45,41° relative to the residues formed from the reagents used in the synthesis (NaCl) and at 29.12 to 29.57° relative to the sodium titanate ($Na_2Ti_9O_{19}$).

The size of the crystallites of the photocatalysts was determined using the Scherrer equation and the intensities of the anatase peaks of each photocatalyst. The results (see Table 2) confirm that the hydrothermal method and the doping with cerium do not change the crystallite size. The doping with Ce inhibits the growth of the crystallite even when the material is calcined at 600° C and, with a lower concentration of the metal, this advantage is greater [34,47].

3.4. Zeta potential

The stability and point of zero charge of the photocatalysts prepared were analyzed by measuring the zeta potential in an aqueous system using distilled water and compared with pure TiO_2-P25 (see Table 2). A high value for zeta potential (positive or negative) indicates less agglomeration, i.e. more particles will be available for the adsorption of substrate molecules and thus, control the interfacial properties of TiO_2 and hence, the photocatalytic activity [48,49].

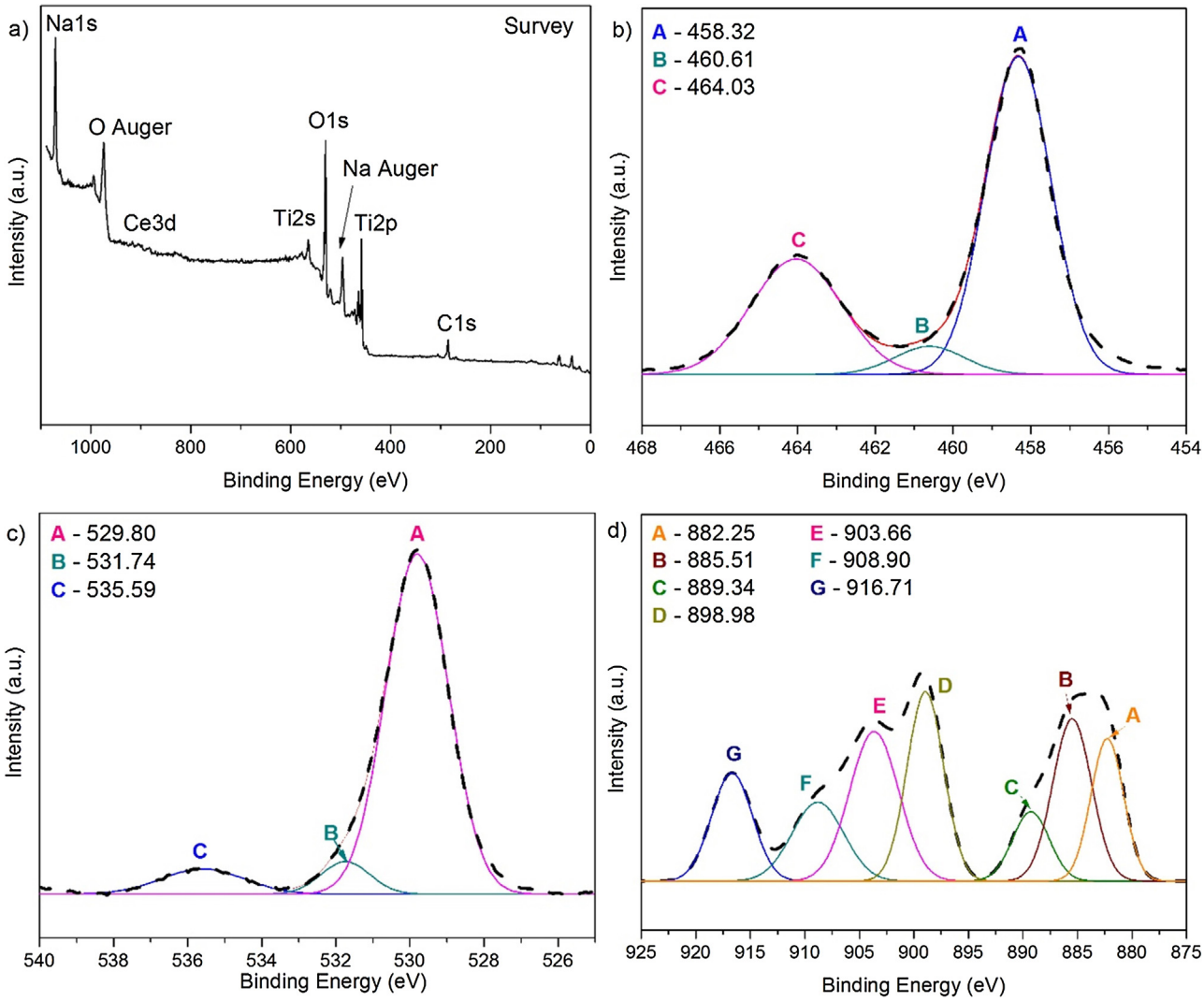

Fig. 4. XPS of 2.9Ce-TiO_2-450: (a) survey spectra, (b) Ti 2p core-level spectra, (c) O 1 s core-level spectra and (d) Ce 3d core-level spectra.

Table 3
Amount of MB adsorbed on different photocatalysts ($C_0 = 20\ mg\ L^{-1}$; $C_{cat} = 0.5\ g\ L^{-1}$; pH 6.0).

Photocatalysts	Amount of MB adsorbed	
	($mg\ g^{-1}$)	q/S_{BET} ($mg\ m^{-2}$)
TiO_2-P25	1.67	0.03
TiO_2-450	32.91	0.41
TiO_2-600	24.28	0.51
0.09Ce-TiO_2-450	34.75	0.38
0.09Ce-TiO_2-600	26.32	0.58
0.29Ce-TiO_2-450	34.46	0.32
0.29Ce-TiO_2-600	31.75	0.59
0.57Ce-TiO_2-450	33.08	0.45
0.57Ce-TiO_2-600	28.55	0.50

Under the basic conditions of the synthesis, Ce^{3+} is more unstable in the presence of air than Ce^{4+} [50]. So, in the hydrothermal treatment of an aqueous solution of $Ce(NO_3)_3$ the formation of hydrated CeO_2 is expected, and meanwhile OH^- ions were predominately adsorbed onto the surface of CeO_2, giving rise to the existence of a large portion of surface hydroxyls for the CeO_2 nanoparticles obtained on the TiO_2 surface. In general, TiO_2 photocatalysts prepared by the hydrothermal method had a low point of zero charge (pHpzc), due to the treatment with 10 M NaOH [51,52], which improves the amount of OH groups on the solid surface. The calcination temperature modifies the morphology and surface area of the material, which winds up interfering with its zero load point [53], as shown in Table 2, but no significant interference on the Ce content was found.

3.5. Evidence of Ce doped TiO_2 and cerium valence state by XPS

The Ce doped TiO_2 photocatalysts prepared by the hydrothermal method were analyzed by XPS to understand the change in the chemical bonding of the surface caused by the cerium doping of the titanium dioxide structure, as well as the position of the electronic valence band of Ti and Ce. Since a percentage of 0.29% of Ce is very low for detection in the equipment, a sample of TiO_2 doped with 2.9% Ce calcined at 450 °C was prepared for analysis. In fact, it is a challenge to detect Ce 4f states with regular XPS in low Ce content CeO_x-TiO_2 samples [11].

Fig. 4a shows the XPS survey spectrum of 2.9Ce-TiO_2-450, where we observed the presence of Na, which comes from the reagents used to prepare the photocatalyst.

Fig. 4b is the Ti 2p core-level XPS spectra, which shows the presence of Ti^{4+}. The binding energies of the peaks are found to be at 464.03 eV for Ti $2p_{1/2}$ and 458.32 eV for Ti $2p_{3/2}$, which are in agreement with the binding energies of TiO_2 reported earlier in the literature. The peak at 460.61 eV refers to O1s excited by AlKα radiation.

Fig. 4c shows the binding states of oxygen in 2.9Ce-TiO_2-450 with the O 1s XPS peak fitted to three deconvoluted peaks. Peaks A (529.80 eV) in Fig. 4c represent the O_2^- ion in the TiO_2 crystal structure and the peak at 531.81 eV is assigned to Ti-OH [15,54]. The dominant peak (A) was characteristic of the metal oxides arising from the lattice of ceria and titanium [42,55]. The peak (C) at 535.59 eV refers to the Auger peak of sodium (Na KLL). The characteristic peaks of the Na compounds found in XRD and XPS analyses are of low intensity, showing that there is a very small amount of residual Na in some of the samples analyzed. Therefore, its presence should have no effect on photocatalytic tests.

The Ce 3d labels in Fig. 4d refer to the $3d_{5/2}$ and $3d_{3/2}$ spin orbital [42]. The peaks located close to 882.25 eV and 898.98 eV can be attributed to the Ce $3d_{5/2}$ and Ce $3d_{3/2}$, respectively [56]. The oxidative Ce is a mixture of Ce^{3+} and Ce^{4+}. The appearance of signals at 882.34, 898.98 eV is evidence of the presence of Ce^{4+} [57,58]. The satellite peak at 916.71 eV is a fingerprint of Ce^{4+} compounds. However, the intensity of this component is not proportional to the amount of Ce^{4+} states [56]. The peaks at 889.34 and 908.90 eV refer to Ce^{3+} and are attributed to the interaction between ceria and the surrounding atoms. They can be used as indicators of the existence of oxygen vacancies [59]. The other signals, located at about 885.51 and 903.66 eV, indicate the existence of Ce [54].

The nominal relationship between Ce:Ti was compared with that measured by XPS analysis for the sample 2.9Ce-TiO_2-450 and the results showed that cerium atoms are well dispersed on the solid surface. While the nominal Ce:Ti ratio is 0.029, the measured Ce:Ti ratio is 0.026, indicating that the hydrothermal method was efficient for conducting the doping.

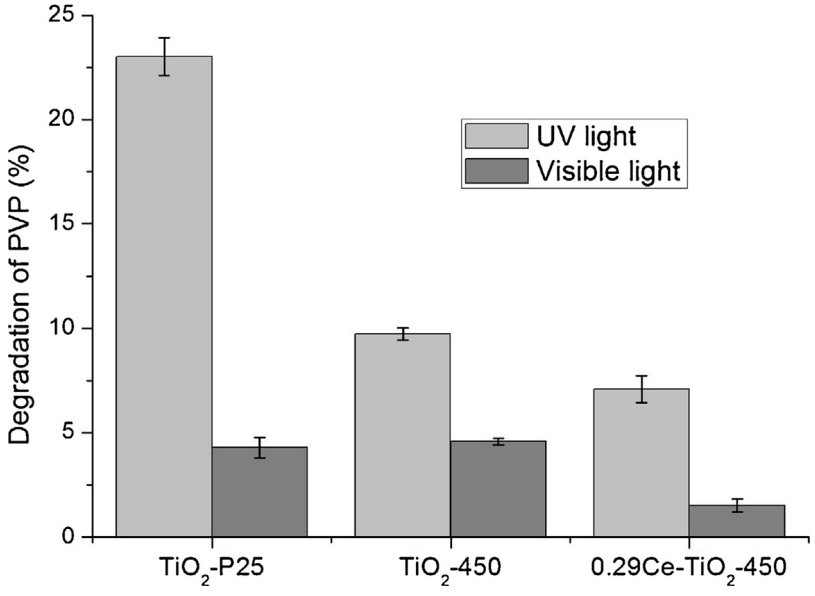

Fig. 5. Photocatalytic degradation of polymer PVP under visible and UV light; using different photocatalysts after 4 h reaction ($C_0 = 300\ mg\ L^{-1}$; $C_{cat} = 500\ mg\ L^{-1}$).

3.6. Adsorption capacity

Preliminary tests showed that there is no PVP adsorption on the surface of the photocatalysts under dark conditions, probably due to the complex nature of the polymer and its molecular weight, which is very high, and because it is much larger than the pores available on the surface of the photocatalysts. In addition, their zeta potentials are similar, resulting in incompatibility of charges. On the other hand, a high quantity of MB is adsorbed, as shown in Table 3.

It is observed that the extension of the surface area determines the amount of MB adsorbed, and is nearly independent from the cerium surface density (Tables 2 and 3).

The MB solution had an initial pH of 8.4, which is higher than the zero charge point of all the photocatalysts. During adsorption pH decreased to 6.0. Under these conditions, except TiO_2 P25, all other photocatalysts should present a negatively charged surface (pH > pHpzc), which could explain the high amount of the cationic molecule of MB adsorbed.

The adsorption of the MB on the photocatalyst surface plays an important role in the photocatalytic degradation process [60,61]. As shown in Table 3, the amount of MB adsorbed is nearly the same for all samples prepared, and it is much higher than that using TiO_2 P25. The changes in morphology and electrical aspects from the solid-liquid interface are responsible for the increase in the adsorption capacity of MB on the photocatalysts prepared in this work.

3.7. Photodegradation of PVP under visible or UV light

The results of photocatalytic degradation of PVP under visible or UV light (Fig. 5) showed that the prepared photocatalysts have lower activity than TiO_2-P25 under UV light, even the high surface area Ce doped TiO_2. Since PVP is not adsorbed on the solid surface, it seems that the photogeneration of e^-/h^+ pairs and further hydroxyl radicals' generation are the main factors responsible for the PVP degradation [33].

Because the adsorption capacity of the PVP on the photocatalysts used in this work is negligible, due to the high molecular size and low affinity of PVP, no effect was observed for Ce doping on the degradation of PVP under UV light (Fig. 6).

As shown in Fig. 6, the •OH scavenger greatly decreases the degradation of PVP when using TiO_2-P25, and a smaller inhibition was observed when TiO_2-450 was used. So, it is expected that TiO_2-450 will form a smaller amount of •OH by means of oxidation of the water molecule in relation to the other catalysts studied, as well as other radical species like singlet oxygen $^1O_2$.

PVP polymer degradation tests were also carried out with the use of radical scavengers under UV light (NaN_3 as $^1O_2$ scavenger and Na_2CO_3 as the •OH scavenger). The kinetic of PVP degradation follows a pseudo first order reaction [33], and Fig. 6 shows the pseudo-first order kinetic constant for PVP degradation under UV light using different photocatalysts with the presence or absence of radical scavengers. TiO_2-P25 is the most active photocatalyst under UV light and when an •OH scavenger is used (Na_2CO_3), the degradation is greatly inhibited, while the prepared photocatalysts act in degradation predominantly through the singlet oxygen [62,63].

3.8. Photodegradation of MB under visible or UV light

After the adsorption study, the photocatalytic activity of the photocatalysts was evaluated by photodegradation of the MB (Fig. 7).

Table 4 shows the rate constant based on the volume ($k_{1\text{-}v}$). We also evaluted the rate constant based on the amount of catalyst during the catalytic tests ($k_{1\text{-}w}$) [64].

The experiments under visible light showed that the pure TiO_2 photocatalysts prepared by the hydrothermal method have a much higher photocatalytic activity than TiO_2-P25 in the degradation of MB under visible light. This can be explained by the morphology modified by the hydrothermal method, which provides the TiO_2 a high surface area and an elongated shape (see Fig. 1) that could increase its conductivity, increasing the electron transfer and consequently decreasing the recombination of the photogenerated pairs under visible light.

The highest photocatalytic activity under UV light was found for the TiO_2-P25 (0.080 min^{-1}) because of its high ability to produce •OH radicals. The prepared photocatalysts (doped and undoped) have a higher adsorption capacity and the large amount of MB present on their surfaces impairs the formation of hydroxyl

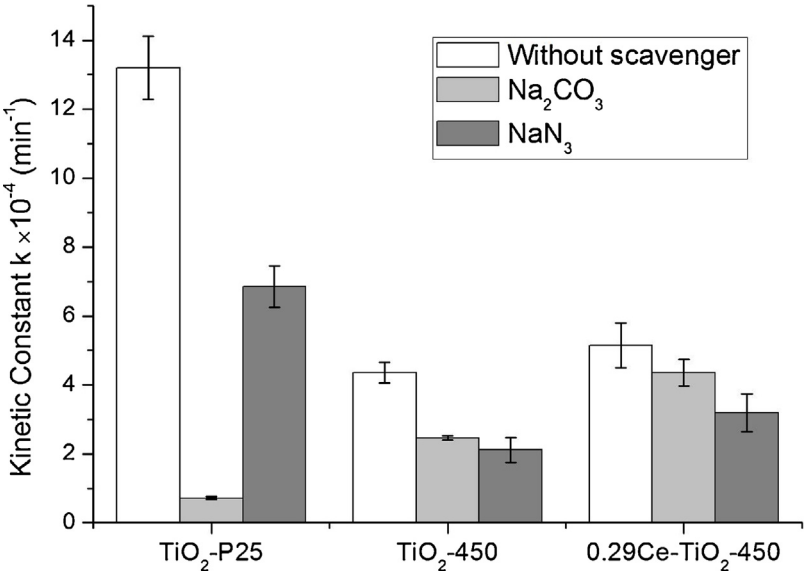

Fig. 6. Pseudo-first order kinetic constant of the degradation of polymer PVP by TiO_2-P25, TiO_2-450, 0.29Ce-TiO_2-450 in the presence of ROS scavengers under UV light (C_0=300 mg L^{-1}; C_{cat}=500 mg L^{-1}; C_{sca} = 5 mM).

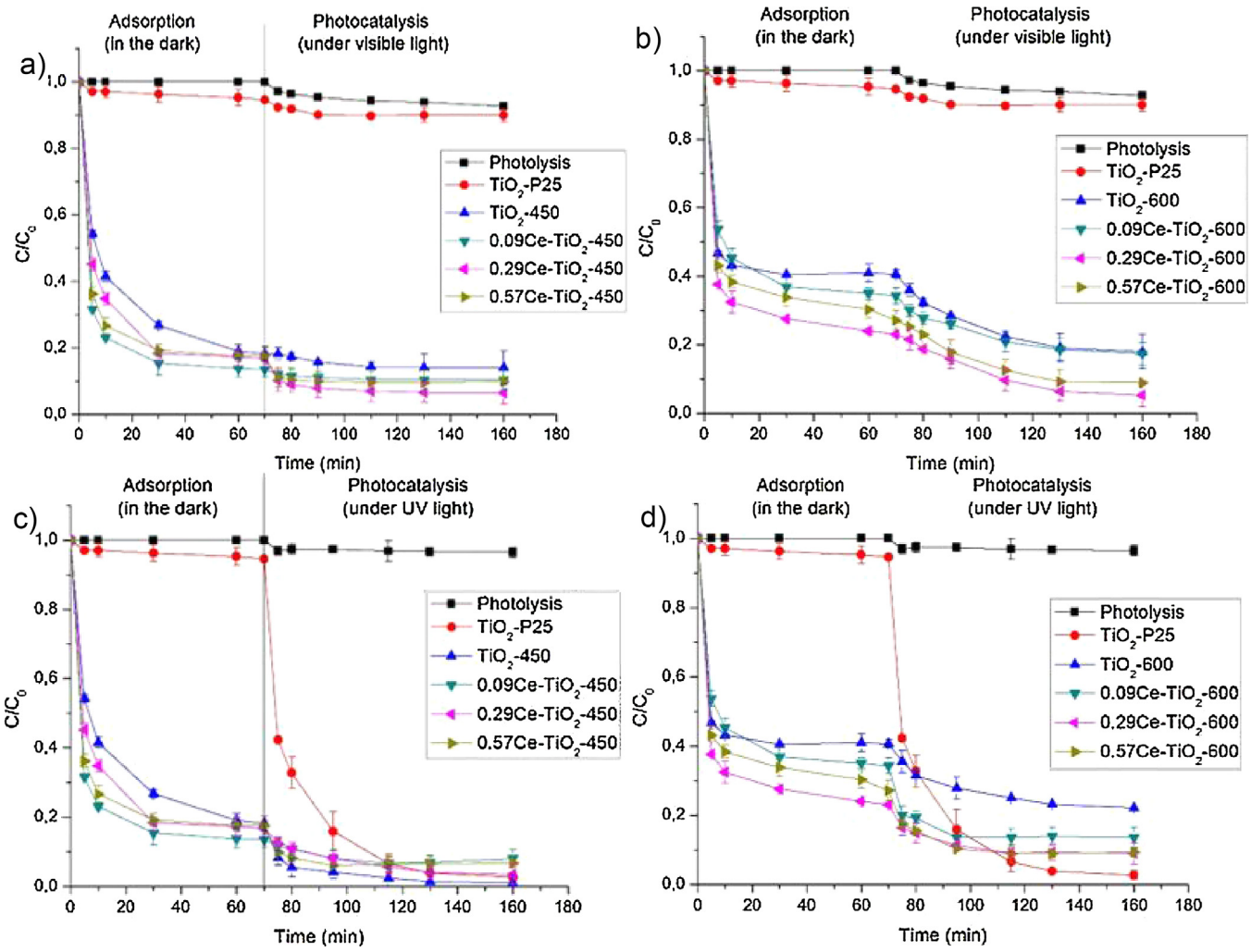

Fig. 7. Photocatalytic degradation of MB by the photocatalysts under visible (a–b) and UV (c–d) light. (C_0=20 mg L^{-1}, C_{cat} = 500 mg L^{-1}).

Table 4
Pseudo-first order kinetic constant for MB photodegradation under visible and UV light for photocatalysts.

Light	Photocatalysts	$k_{1\text{-}v}$ (min^{-1})	$k_{1\text{-}w}$ ($L g_{cat}^{-1} min^{-1}$)
Visible	TiO_2-P25	0.00249 ± 0.00028	0.00498 ± 0.00056
	TiO_2-450	0.01734 ± 0.00114	0.03468 ± 0.00228
	TiO_2-600	0.00703 ± 0.00059	0.01406 ± 0.00118
	0.09Ce-TiO_2-450	0.00458 ± 0.00021	0.00916 ± 0.00042
	0.09Ce-TiO_2-600	0.00213 ± 0.00025	0.00426 ± 0.00050
	0.29Ce-TiO_2-450	0.02143 ± 0.00169	0.04286 ± 0.00338
	0.29Ce-TiO_2-600	0.00381 ± 0.00017	0.00762 ± 0.00034
	0.57Ce-TiO_2-450	0.01131 ± 0.00161	0.02262 ± 0.00322
	0.57Ce-TiO_2-600	0.00499 ± 0.00014	0.00998 ± 0.00028
UV	TiO_2-P25	0.08087 ± 0.00848	0.16174 ± 0.01696
	TiO_2-450	0.05715 ± 0.00328	0.11430 ± 0.00656
	TiO_2-600	0.05425 ± 0.00165	0.10850 ± 0.00330
	0.09Ce-TiO_2-450	0.04034 ± 0.00247	0.08068 ± 0.00494
	0.09Ce-TiO_2-600	0.03308 ± 0.00096	0.06616 ± 0.00192
	0.29Ce-TiO_2-450	0.03244 ± 0.00245	0.06488 ± 0.00490
	0.29Ce-TiO_2-600	0.03096 ± 0.00146	0.06192 ± 0.00292
	0.57Ce-TiO_2-450	0.04875 ± 0.00485	0.09750 ± 0.00970
	0.57Ce-TiO_2-600	0.04800 ± 0.00390	0.09600 ± 0.00780

radicals and facilitates the formation of singlet oxygen through the photogenerated holes.

Among the photocatalysts doped with cerium, the highest photocatalytic activity under visible light was found for the solid with the highest surface area (0.29Ce-TiO_2-450). On the other hand, under UV light the photocatalytic activity seems to depend on the band gap energy, because 0.57Ce-TiO_2-450 was the more active Ce-doped photocatalyst. The results obtained in this study were similar to those obtained by other authors [5,65]. Futhermore, no relationship was observed between the MB degradation and Ce_{sd} (Tables 2 and 4).

The identification of the main reactive oxygen species produced on the photocatalytic surface and that are involved in the MB degradation was investigated using TiO_2-P25, TiO_2-450 and 0.29Ce-TiO_2-450. It is well-known that the hydroxyl radical ($^{\bullet}OH$) is a very strong oxidant and is the dominant species in the photocatalytic process [1,3,62]. In the absence of suitable electron acceptors, recombination is extremely efficient and thus represents a great loss of energy, limiting the achievement of a high quantum yield. However, other reactive oxygen species (ROS) could be involved in the MB degradation (Eqs. (7)–(11)), such as $^1O_2$, $^{\bullet}OH$, O_2H, etc.

$$\text{Photocatalyst} + h\nu \rightarrow h^+ + e^- \quad (7)$$

$$O_2 + e^- \rightarrow O_2^{\circ -} \quad (8)$$

$$h^+ + O_2^{\circ -} \rightarrow {}^1O_2 \quad (9)$$

$$h^+ + H_2O \rightarrow {}^{\circ}OH \quad (10)$$

$$ROS + MB \rightarrow Intermediates \rightarrow CO_2 + H_2O \quad (11)$$

To further study the photocatalytic process, a comparison of the photocatalytic activity in the presence of radical scavengers was carried out using L-Histidine as the $^1O_2$ scavenger and DMSO as the $^{\bullet}OH$ scavenger. The results are displayed in Fig. 8.

The results from Fig. 8a reveals that the addition of DMSO has a negative influence on the degradation efficiency of MB, indicating that DMSO can consume $^{\bullet}OH$ in aqueous solution to block the photocatalytic reaction under UV light. These results suggest that $^{\bullet}OH$ was partially responsible for the photooxidation using TiO_2 P25, as largely confirmed by the literature.

Fig. 8a shows that in the absence of any radical scavenger the photocatalysts studied have a higher kinetic velocity constant than when there is withdrawal of some ROS from the reaction, with TiO_2-P25 being the most active under UV light. The kinetic velocity constant of the degradation of MB using the cerium doped photocatalyst undergoes greater influence when using L-Histidine (singlet oxygen scavenger). It is known that $^{\bullet}OH$ has a higher oxidizing power, but is more prone to loss of efficiency in aqueous complexes. $^1O_2$ is more selective and less affected in the presence of organic matter [66].

On the other hand, the effect of adding scavengers is quite different under visible light (Fig. 8b), with 0.29Ce-TiO_2-450 being the most active photocatalyst. This could be related to its high BET surface area (Table 2) and high contact between ceria and titania, which results in a high adsorption capacity and may facilitate the transfer of an electron from the MB aromatic rings to the photogenerated gap on the surface of the photocatalysts. The lower adsorption capacity of MB at the surface of TiO_2-P25 would imply the occurrence of the oxidation reaction of adsorbed water to produce $^{\bullet}OH$ radicals. Thus, there would be greater inhibition of MB degradation using TiO_2-P25 than with the materials prepared.

The addition of L-Histidine, which acts as a singlet oxygen radical scavenger, almost completely inhibited the reaction of MB on photocatalysts (doped or non-doped), indicating that the mechanism of degradation occurs via a reaction with the oxygen radicals produced in the conduction band by the reaction of the dissolved oxygen with the photogenerated electrons. The MB reaction using TiO_2-P25 undergoes less inhibition, indicating that almost all photogenerated free radicals ($^{\bullet}OH$, $O_2^{\bullet-}$, $^{\bullet}O_2H$, h^+) are involved in the degradation.

During the photocatalysis irradiated under visible light, Fig. 8b, two types of mechanisms could be involved: a direct mechanism, by the action of a photogenerated gap as the oxidant through electron transfer (Eqs. (12)–(15)) or an indirect mechanism, by the action of $^{\bullet}OH$ radicals by abstracting H atoms of the organic molecule or adding to the double C=C bonds present in the molecule (Eqs. (7)–(11)) [67]. The latter can occur on the catalyst surface or in solution, in both cases the electron is injected from the excited dye molecule adsorbed on the catalyst surface into the conduction band of the photocatalyst. Thus, the electron that is trapped by the molecular oxygen present on the photocatalyst surface generates highly active radicals that are responsible for the photodegradation of MB molecules. The photocatalysis sensitized by the dye on the TiO_2 surface may be promoted following the reactions

$$dye + hv \rightarrow dye^* \quad (12)$$

$$dye^* + TiO_2 \rightarrow dye^{\circ+} + TiO_2(e^-) \quad (13)$$

$$TiO_2(e^-) + O_2 \rightarrow TiO_2 + O_2^{\circ-}(ROS) \quad (14)$$

$$dye^{\circ+} + O_2^{\circ-} \rightarrow \text{degraded products} \rightarrow CO_2 + H_2O \quad (15)$$

One of the main factors that affect the performance of a catalyst in the degradation process is the surface area, because the larger the surface area the greater will be the adsorption and thus the greater the degradation [13]. The surface area extension increased adsorption capacity (see Tables 2 and 3) and the degradation rate of MB under visible light, since the most active photocatalyst (0.29Ce-TiO_2-450) was that with the highest BET surface area. Therefore, a suitable Ce content could guarantee the maintenance of the surface area extension during the synthesis.

A large amount of adsorbed dye on the photocatalyst surface irradiated by visible light increases the photocatalytic degradation of MB by dye-sensitized Ce-TiO_2 under visible-light irradiation [68]. The effective contact between ceria and titania could influence the activity by promoting an effective separation of charge and leaving holes species available for adsorption and chemical reaction.

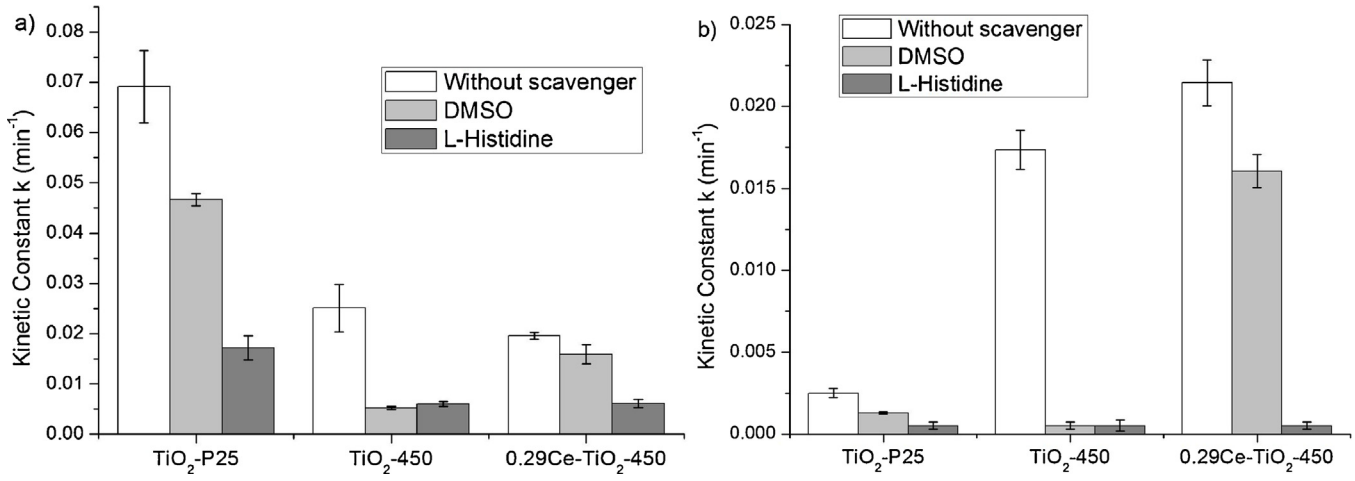

Fig. 8. Pseudo-first order kinetic constant of the degradation of MB by TiO_2-P25, TiO_2-450, 0.29Ce-TiO_2-450 in the presence of ROS scavengers under (a) UV and (b) visible light (C_0 is the last adsorption point for each reaction; C_{cat} = 500 mg L^{-1}; C_{sca} = 5 mM).

4. Conclusions

The change in the TiO_2 morphology using the hydrothermal method increased the surface area of the photocatalysts, which increased their adsorption capacity. The adsorption of MB is easier than that of PVP due to the size of the molecule and the isoelectric potential of the photocatalysts. Cerium doping promoted greater stability of TiO_2 even at high temperatures, which offers greater advantages when applied by industry.

Doping TiO_2 with Ce is not efficient for the degradation of complex matrix compounds, such as PVP, but it becomes an efficient photocatalyst in the photodegradation of simple compounds, such as MB dye, which is easily adsorbed. The higher concentration of MB on the photocatalyst's surface mediates the activation of the TiO_2, modifying the degradation mechanism of the compound. This was proven when the rate of degradation of MB by the Ce-doped photocatalyst decreased dramatically when using a singlet oxygen scavenger, under visible and UV light. In addition, there was no degradation of the PVP polymer, because the complex matrix compound is not adsorbed on the surface of the photocatalyst. This proves that cerium doped photocatalysts clearly work to degrade dyes through sensitized photocatalysis.

Acknowledgments

This study was supported by the National Council for Technological and Scientific Development(CNPq/Brazil) and the Coordination for the Improvement of Higher Education Personnel (CAPES/Brazil), as well as by other partners at UFSC (LCME, LFFS and CERMAT); UFPR (Prof. Dr. Wido H. Schreiner) and UNICAMP (Prof. Dr. Richard Landers).

References

[1] A. Mills, S.L. Hunte, An overview of semiconductor photocatalysis, J. Photochem. Photobiol. A 108 (1997) 1–35.
[2] M.J. Muñoz-Batista, M.N. Gómez-Cerezo, A. Kubacka, D. Tubela, M. Fernández-Garcia, Role of interface contact in CeO_2-TiO_2 photocatalytic composite materials, ACS Catal. 4 (2014) 63–72.
[3] J.-M. Herrmann, Fundamentals and misconceptions in photocatalysis, J. Photochem. Photobiol. A 216 (2010) 85–93.
[4] C.L. Bianchi, E. Colombo, S. Gatto, M. Stucchi, G. Cerrato, S. Morandi, V. Capucci, Photocatalytic degradation of dyes in water with micro-sized TiO_2 as powder or coated on porcelain-grès tiles, J. Photochem. Photobiol. A 180 (2014) 27–31.
[5] C. Belver, J. Bedia, M.A. Álvarez-Montero, J.J. Rodriguez, Solar photocatalytic purification of water with Ce-doped TiO_2/clay heterostructures, Catal. Today 266 (2016) 36–45.
[6] Á. Kukovecz, K. Kordás, J. Kiss, Z. Kónya, Atomic scale characterization and surface chemistry of metal modified titanate nanotubes and nanowires, Surf. Sci. Rep. 71 (2016) 473–546.
[7] N. Coleman Jr., S. Perera, E.G. Gillan, Rapid solid-state metathesis route to transition-metal doped titanias, J. Solid State Chem. 232 (2015) 241–248.
[8] M. Jovaní, M. Domingo, T.R. Machado, E. Longo, H. Beltrán-Mir, E. Cordocillo, Pigments based on Cr and Sb doped TiO_2 prepared by microemulsion-mediated solvothermal synthesis for inkjet printing on ceramics, Dyes Pigm. 116 (2015) 106–113.
[9] J. Reszczyñska, T. Grzyb, J.W. Sobczak, W. Lisowski, M. Gazda, B. Ohtani, A. Zaleska, Visible light activity of rare earth metal doped (Er^{3+}, Yb^{3+} or Er^{3+}/Yb^{3+}) titania photocatalysts, Appl. Catal. B—Environ. 163 (2015) 40–49.
[10] C. Zhan, F. Chen, J. Yang, D. Dai, Visible light responsive sulfated rare earth doped TiO_2@fumed SiO_2 composites with mesoporosity: enhanced photocatalytic activity for methyl orange degradation, J. Hazard. Mater. 267 (2014) 88–97.
[11] S. Luo, T.-D. Nguyen-Phan, A.C. Johnston-Peck, L. Barrio, S. Sallis, D.A. Arena, S. Kundu, W. Xu, L.F.J. Piper, E.A. Stack, D. Polyanskiy, E. Fujita, J.A. Rodriguez, S.D. Senanayake, Hierarchical heterogeneity at the CeO_xTiO_2 interface: electronic and geometrical structural influence on the photocatalytic activity of oxide on oxide nanostructures, J. Phys. Chem. 119 (2015) 2669–2679.
[12] F. Galindo-Hernández, R. Gómez, Degradation of the herbicide 2,4-dichlorophenoxyacetic acid over TiO_2–CeO_2 sol–gel photocatalysts: effect of the annealing temperature on the photoactivity, J. Photochem. Photobiol. A 217 (2011) 383–388.
[13] A. Rapsomanikis, A. Apostolopoulou, E. Stathatos, P. Lianos, Cerium-modified TiO_2 nanocrystalline films for visible light photocatalytic activity, J. Photochem. Photobiol. A 280 (2014) 46–53.
[14] W. Xue, G. Zhang, X. Xu, X. Yang, C. Liu, Y. Xu, Preparation of titania nanotubes doped with cerium and their photocatalytic activity for glyphosate, Chem. Eng. J. 167 (2011) 397–402.
[15] Y. Liu, P. Fang, Y. Cheng, Y. Gao, F. Chen, Z. Liu, Y. Dai, Study on enhanced photocatalytic performance of cerium doped TiO_2-based nanosheets, Chem. Eng. J. 219 (2013) 478–485.
[16] L. Matejová, K. Kocí, M. Reli, L. Capek, A. Hospodková, P. Peikertová, Z. Matej, L. Obalová, A. Wach, P. Kustrowski, A. Kotarba, Preparation characterization and photocatalytic properties of cerium doped TiO_2: On the effect of Ce loading on the photocatalytic reduction of carbon dioxide, Appl. Catal. B—Environ. 152–153 (2014) 172–183.
[17] L. Barrio, G. Zhou, I.D. Gonzalez, M. Estrella, J. Hanson, J.A. Rodriguez, R.M. Navarro, J.L.G. Fierro, In situ characterization of Pt catalysts supported on ceria modified TiO_2 for WGS reaction: influence of ceria loading, Phys. Chem. Chem. Phys. 14 (2012) 2192–2202.
[18] J. Fang, H. Bao, B. He, F. Wang, D. Si, Z. Jiang, Z. Pan, S. Wei, W. Huang, Interfacial and surface structure of CeO_2–TiO_2 mixed oxides, J. Phys. Chem. C 111 (2007) 19078–19085.
[19] H. Gao, B. Qiao, T. Wang, D. Wang, Y. Jin, Cerium oxide coating of titanium dioxide pigment to decrease its photocatalytic activity, Ind. Eng. Chem. Res. 53 (2014) 189–197.
[20] D.A. Andersson, S.I. Simak, N.V. Skorodumova, A.I. Abrikosov, B. Johansson, Redox principles of CeO_2-MO_2 (M = Ti Zr, Hf, or Th) solid solutions from first principles calculations, Appl. Phys. Lett. 90 (2007) 031909.
[21] Z. Bian, J. Zhu, H. Li, Solvothermal alcoholysis synthesis of hierarchical TiO_2 with enhanced activity in environmental and energy photocatalysis, J. Photochem. Photobiol. C 28 (2016) 72–86.
[22] Z. Wu, Q. Wu, L. Du, C. Jiang, L. Piao, Progress in the synthesis and applications of hierarchical flower-like TiO_2 nanostructures, Particuology 15 (2014) 61–70.
[23] Q. Zhou, J. Li, Z. Fang, M. Wang, Applications of TiO_2 nanotube arrays in environmental and energy fields: a review, Microporous Mesoporous Mater. 202 (2015) 22–35.
[24] W. Zhou, Y. He, Ho/TiO_2 nanowires heterogeneous catalyst with enhanced photocatalytic properties by hydrothermal synthesis method, Chem. Eng. J. 179 (2011) 412–416.
[25] H. Cai, X. Chen, Q. Li, B. He, Q. Tang, Enhanced photocatalytic activity from Gd. La codoped TiO_2 nanotube array photocatalysts under visible-light irradiation, Appl. Surf. Sci. 284 (2013) 837–842.
[26] N. Wetchakun, B. Incessungvorn, K. Wetchakun, S. Phanichphant, Influence of calcination temperature on anatase to rutile phase transformation in TiO_2 nanoparticles synthesized by the modified sol-gel method, Mater. Lett. 82 (2012) 195–198.
[27] D.A.H. Hanaor, C.C. Sorrell, Review of the anatase to rutile phase transformation, J. Mater. Sci. 46 (2011) 855–874.
[28] D. Rafieian, W. Ogieglo, T. Savenije, R.G.H. Lammertink, Controlled formation of anatase and rutile TiO_2 films by reactive magnetron sputtering, AIP Adv. 5 (2015) (097168-1).
[29] F. Vrantny, S. Kern, F. Gugliotta, The thermal decomposition of cerium (III) nitrate hydrate, J. Inorg. Nucl. Chem. 17 (1961) 281–285.
[30] W. Li, X. Cui, P. Wang, Y. Shao, D. Li, F. Teng, Enhanced photosensitized degradation of rhodamine B on CdS/TiO_2 nanocomposites under visible light irradiation, Mater. Res. Bull. 48 (2013) 3025–3081.
[31] P.W. Koh, M.H.M. Hatta, S.T. Ong, L. Yuliati, S.L. Lee, Photocatalytic degradation of photosensitizing and non-photosensitizing dyes over chromium doped titania photocatalysts under visible light, J. Photochem. Photobiol. A 323 (2017) 215–223.
[32] E.T. Yun, H.Y. Yoo, W. Kim, H.E. Kim, G. Kang, H. Lee, S. Lee, T. Park, C. Lee, J.H. Kim, J. Lee, Visible-light-induced activation of periodate that mimics dye-sensitization of TiO_2: simultaneous decolorization of dyes and production of oxidizing radicals, Appl. Catal. B—Environ. 203 (2017) 475–484.
[33] J. Suave, H.J. José, R.F.P.M. Moreira, Photocatalytic degradation of polyvinylpyrrolidone in aqueous solution using TiO_2/H_2O_2/UV system, Environ. Technol. 29 (2017) 1–9.
[34] M. Meksi, H. Kochkar, G. Berhault, C. Guillard, Effect of cerium content and post-thermal treatment on doped anisotropic TiO_2 nanomaterials and kinetic study of the photodegradation of formic acid, J. Mol. Catal. A—Chem. 409 (2015) 162–170.
[35] L.Z. Pei, H.D. Liu, N. Lin, H.Y. Yu, Hydrothermal synthesis of cerium titanate nanorods and its application in visible light photocatalysis, Mat. Res. Bull. 61 (2015) 40–46.
[36] Y. Xu, C. Chen, X. Yang, X. Li, B. Wang, Preparation, characterization and photocatalytic activity of neodymium-doped TiO_2 nanotubes, Appl. Surf. Sci. 255 (2009) 8624–8628.
[37] M. Reli, N. Ambrožová, M. Šihor, L. Matějová, L. Čapek, L. Obalová, Z. Matěj, A. Kotarba, K. Kočí, Novel cerium doped titania catalysts for photocatalytic decomposition of ammonia, Appl. Catal. B—Environ. 178 (2015) 108–116.
[38] K. Chen, S. Xie, E. Iglesia, A.T. Bell, Structure and properties of zirconia-supported molybdenum oxide catalysts for oxidative dehydrogenation of propane, J. Catal. 189 (2000) 421–430.
[39] B. Ohtani, Photocatalysis A to Z –What we know and what we do not know in a scientific sense, J. Photochem. Photobiol. C 11 (2010) 157–178.
[40] Y. Huang, C.-F. Yan, C.-Q. Guo, Y. Shi, Experimental and first-principles DFT study on oxygen vacancies on cerium dioxide and its effect on enhanced photocatalytic hydrogen production, Int. J. Hydrogen Energy 41 (2016) 7919–7926.

[41] M. Fronzi, A. Iwaswuk, A. Lucid, M. Nolan, Metal oxide nanocluster-modified TiO_2 as solar activated photocatalyst materials, J. Phys. Condens. Matter 28 (2016) 074006 (23pp).
[42] H. Abdullah, M.R. Khan, M. Pudukudy, Z. Yaakob, N.A. Ismail, CeO_2-TiO_2 as a visible light active catalyst for the photoreduction of CO_2 to methanol, J. Rare Earth 33 (2015) 1155–1161.
[43] H. Liu, M. Wang, Y. Wang, Y. Liang, W. Cao, Y. Su, Ionic liquid-templated synthesis of mesoporous CeO_2–TiO_2 nanoparticles and their enhanced photocatalytic activities under UV or visible light, J. Photochem. Photobiol. A 223 (2011) 157–164.
[44] Y.-H. Xu, Z.-X. Zeng, The preparation, characterization, and photocatalytic activities of Ce–TiO_2/SiO_2, J. Mol. Catal. A 279 (2008) 77–78.
[45] Z.M. El-Bahy, A.A. Ismail, R.M. Mohamed, Enhancement of titania by doping rare earth for photodegradation of organic dye (Direct Blue), J. Hazard. Mater. 166 (2009) 138–143.
[46] B. Choudhury, B. Borah, A. Choudhury, Ce-Nd cooping effect on the structural and optical properties of TiO_2 nanoparticles, Mater. Sci. Eng. B 178 (2013) 239–247.
[47] C. Wang, Y. Ao, P. Wang, J. Hou, J. Qian, Preparation, characterization and photocatalytic activity of the neodymium-doped TiO_2 hollow spheres, Appl. Surf. Sci. 257 (2010) 227–231.
[48] E. Morgado Jr., M.A.S. de Abreu, O.R.C. Pravia, B.A. Marinkovic, P.M. Jardim, F.C. Rizzo, A.S. Araújo, A study on the structure and thermal stability of titanate nanotubes as a function of sodium content, Solid State Sci. 8 (2006) 888–900.
[49] I.S. Grover, S. Singh, B. Pal, The preparation, surface structure, zeta potential, surface charge density and photocatalytic activity of TiO_2 nanostructures of different shapes, Appl. Surf. Sci. 280 (2013) 366-372.
[50] T. Cao, Y. Li, C. Wang, L. Wei, C. Shao, Y. Liu, Fabrication structure, and enhanced properties of hierarchical CeO_2 nanostructures/TiO_2 nanofibers heterostructures, Mater. Res. Bull. 45 (2010) 1406–1412.
[51] J. Yu, H. Yu, B. Cheng, C. Trapalis, Effects of calcination temperature on the microstructures and photocatalytic activity of titanate nanotubes, J. Mol. Catal. A—Chem. 249 (2006) 135–142.
[52] M. Sahu, P. Biswas, Single-step processing of copper-doped titania nanomaterials on a flame aerosol reactor, Nanoscale Res. Lett. 6 (2011) 441–454.
[53] E.M. Hotze, T. Phenrat, G.V. Lowry, Nanoparticle aggregation: challenges to understanding transport and reactivity in the environment, J. Environ. Qual. 39 (2010) 1909–1924.
[54] Y. Tan, S. Zhang, K. Liang, Photocurrent response and semiconductor characteristics of Ce-Ce_2O_3-CeO_2-modified TiO_2 nanotubes arrays, Nanoscale Res. Lett. 9 (2014) 67–72.
[55] N. Aman, P.K. Satapathy, T. Mishra, M. Mahato, N.N. Das, Synthesis and photocatalytic activity of mesoporous cerium doped TiO_2 as visible light sensitive photocatalyst, Mater. Res. Bull. 47 (2012) 179–183.
[56] E. Bêche, P. Charvin, D. Perarnau, S. Abanades, G. Flamant, Ce 3d XPS investigation of cerium oxides and mixed cerium oxide ($Ce_xTi_yO_z$), Surf. Interface Anal. 40 (2008) 264–267.
[57] Y. Cheng, M. Zhang, G. Yao, L. Yang, J. Tao, Z. Gong, G. He, Z. Sun, Band gap manipulation of cerium doping TiO_2 nanopowders by hydrothermal method, J. Alloys Compd. 662 (2016) 179–184.
[58] M. Engelhard, S. Azad, C.H.F. Peden, S. Thevuthasan, X-ray photoelectron spectroscopy studies of oxidized and reduced CeO_2(111) surfaces, Surf. Sci. Spectra 11 (2004) 73–81.
[59] M.A. Henderson, C.L. Perkins, M.H. Engelhard, S. Thevuthasan, C.H.F. Peden, Redox properties of water on the oxidized and reduced surfaces of CeO_2(111), Surf. Sci. 526 (2003) 1–18.
[60] G. Magesh, B. Viswanathan, R.P. Viswanathan, T.K. Varadarajan, Photocatalytic behavior of CeO_2-TiO_2 system for the degradation of methylene blue, Indian J. Chem. 48A (2009) 480–488.
[61] A. Turki, C. Guillard, F. Dappozze, G. Berhault, Z. Ksibi, H. Kochkar, Design of TiO2 nanomaterials for the photodegradation of formic acid –Adsorption isotherms and kinetics study, J. Photochem. Photobiol. A 279 (2014) 8–16.
[62] A. Turolla, A. Piazzoli, J.F. Budarz, M.R. Wiesner, M. Antonelli, Experimental measurement and modelling of reactive species generation in TiO_2 nanoparticle photocatalysis, Chem. Eng. J. 271 (2015) 260–268.
[63] S. Horikoshi, H. Hidaka, N. Serpone, Photocatalyzed degradation of polymers in aqueous semiconductor suspensions V. Photomineralization of lactam ring-pendant polyvinylpyrrolidone at titania/water interfaces, J. Photochem. Photobiol. A 138 (2001) 69–77.
[64] R. Camposeco, S. Castillo, I. Mejía-Centeno, J. Navarrete, N. Nava, Synthesis of protonated titanate nanotubes tailored by the washing step: effect upon acid properties and photocatalytic activity, J. Photochem. Photobiol. A 341 (2017) 87–96.
[65] Z. Fan, F. Meng, J. Gong, H. Li, Y. Hu, D. Liu, Enhanced photocatalytic activity of hierarchical flower-like CeO_2/TiO_2 heterostructures, Mater. Lett. 175 (2016) 36–39.
[66] J. Brame, M. Long, Q. Li, P. Alvarez, Trading oxidation power for efficiency: differential inhibition of photo-generated hydroxyl radicals versus singlet oxygen, Water Res. 60 (2014) 259–266.
[67] A. Mills, C. O'Rourke, K. Moore, Powder semiconductor photocatalysis in aqueous solution: an overview of kinetics-based reaction mechanisms, J. Photochem. Photobiol. A 310 (2015) 66–105.
[68] Y. Xie, C. Yuan, X. Li, Photosensitized and photocatalyzed degradation of azo dye using Ln^{n+}-TiO_2 sol in aqueous solution under visible light irradiation, Mater. Sci. Eng. B 117 (2005) 325–333.